Standing and Transient Eddies in the Response of the Southern Ocean Meridional Overturning to the Southern Annular Mode

C. Dufour, J. Le Sommer, J. Zika, M. Gehlen, J. Orr, P. Mathiot, B. Barnier

Standing and Transient Eddies in the response of the Southern Ocean Meridional Overturning to the Southern Annular Mode

Carolina O. Dufour, Julien Le Sommer, Jan D. Zika, Marion Gehlen, James C. Orr, Pierre Mathiot, Bernard Barnier

Standing and Transient Eddies in the response of the Southern Ocean Meridional Overturning to the Southern Annular Mode

C. O. Dufour *

Laboratoire des Ecoulements Géophysiques et Industriels, CNRS/Université de Grenoble, France

Laboratoire des Sciences du Climat et l'Environnement, CEA-CNRS, France

J. Le Sommer , J. D. Zika

Laboratoire des Ecoulements Géophysiques et Industriels, CNRS/Université de Grenoble, France

M. Gehlen

Laboratoire des Sciences du Climat et l'Environnement/IPSL, CEA-CNRS-UVSQ, France

J. C. Orr

Laboratoire des Sciences du Climat et l'Environnement/IPSL, CEA-CNRS-UVSQ, France

P. Mathiot

Georges Lemaître Center for Earth and Climate Research, Earth and Life Institute, Louvain-la-Neuve, Belgium

B. Barnier

Laboratoire des Ecoulements Géophysiques et Industriels, CNRS/Université de Grenoble, France

---

Corresponding author address: Carolina Dufour, Laboratoire des Ecoulements Géophysiques et Industriels, CNRS/Université de Grenoble, BP53, 38041 Grenoble cedex 9, France.

E-mail: carolina.dufour@hmg.inpg.fr

ABSTRACT

To refine understanding of how Southern Ocean responds to recent intensification of the Southern Annular Mode (SAM), a regional ocean model at two eddy-permitting resolutions was forced with two synthetic interannual forcings. The first forcing corresponds to homogeneously intensified winds, while the second concerns their poleward intensification, consistent with positive phases of the SAM. Resulting wind-driven responses differ greatly between the nearly insensitive Antarctic Circumpolar Current (ACC) and the more sensitive Meridional Overturning Circulation (MOC). As expected, eddies mitigate the response of the ACC and MOC to poleward intensified winds. However, transient eddies do not necessarily play an increasing role in meridional transport with increasing winds and resolution. As winds increase, meridional transport from standing eddies becomes more efficient at balancing wind-enhanced overturning. These results question the current paradigms on the role of eddies and present new challenges for eddy flux parameterization. Results also indicate that spatial patterns of wind anomalies are at least as important as the overall change in intensity in influencing the Southern Ocean's dynamic response to wind events. Poleward intensified wind anomalies from the positive trend in the SAM are far more efficient in accelerating the ACC than homogeneous wind anomalies.

1

1. Introduction

The Southern Annular Mode (SAM) is the dominant mode of atmospheric variability in the Southern Hemisphere. It is characterized by an annular structure centered over Antarctica and is evident in many atmospheric fields. In positive phases of the SAM, the polar vortex contracts, resulting in poleward-intensified zonal winds over the circumpolar ocean (Hall and Visbeck 2002; Sen Gupta and England 2006). Observations reveal a trend in the SAM towards greater dominance of positive phases over the past decades (Thompson et al. 2000; Cai and Whetton 2003; Marshall 2003), a tendency resulting from a non-linear combination of natural and anthropogenic forcing (Thompson and Solomon 2002; Marshall et al. 2004).

Changes in its dynamics are likely to affect the Southern Ocean's capacity as a sink of CO_2 (Metzl et al. 1999; Le Quéré et al. 2007). The response of the Southern Ocean carbon cycle to the upward trend in the SAM is thought to be driven largely by changes in upwelling, which brings deep water that is rich in dissolved inorganic carbon (DIC) to the surface (Lenton and Matear 2007; Lovenduski et al. 2007, 2008). Thus the response is driven by changes in the meridional overturning circulation (MOC).

The MOC cannot be directly deduced from observations though; it must be investigated indirectly, in particular through modeling studies, which can assess the response of the MOC to changes in winds. Along with a poleward intensification of zonal winds, Ekman transport and Ekman pumping are expected to be enhanced and shifted poleward. This would be followed by tightening of isopycnal slopes and poleward shift of isopycnals, resulting in enhanced and poleward shifted Antarctic Circumpolar Current (ACC) transport (Hall and

Visbeck 2002; Spence et al. 2010). Thus the MOC is likely to be enhanced and shifted as well (Sen Gupta and England 2006; Hallberg and Gnanadesikan 2006). Modeling studies indicate that during a positive phase of the SAM, there is an increase in vertical tilt of isopycnals, which intensifies the ACC (Hall and Visbeck 2002; Meredith and Hogg 2006; Yang et al. 2008; Spence et al. 2010; Farneti et al. 2010), and a shift of the ACC poleward by a few degrees (Spence et al. 2010). An acceleration and shift in the position of the ACC coincident with positive phases of the SAM have indeed been reported (e.g. Meredith et al. 2004; Sallée et al. 2008). Likewise, the MOC is shown to intensify and change its structure due to poleward intensification of winds, thus implying substantial changes in properties and rates of formation of water masses (Oke and England 2004; Sen Gupta and England 2006; Hallberg and Gnanadesikan 2006; Naveira Garabato et al. 2009).

In contrast, recent observed trends in isopycnal slopes suggest that ACC transport and the Southern Ocean's MOC may be insensitive to decadal changes in wind stress (Böning et al. 2008). A possible explanation may be the role played by eddies, which have not been accounted for explicitly in studies with coarse-resolution models. Recent studies using high resolution models have shown that eddies may play a major role in the dynamical response of the Southern Ocean to the SAM (Hallberg and Gnanadesikan 2006; Farneti et al. 2010). Indeed, eddies are thought to counteract the steepening of isopycnal slopes induced by the increase in Ekman transport. The MOC's response to changes in winds is also thought to be largely moderated by eddies (Hallberg and Gnanadesikan 2006; Farneti et al. 2010).

It has been proposed that the apparent discrepancy between the results of coarse-resolution models and the limited observations, is due to the inability of such models to resolve eddies. Resolving eddies, not simply parameterizing their effect, may be crucial when studying

3

the response of the Southern Ocean to changes in the SAM. However, if this latter point has clearly emerged from the recent literature, little is known as for the respective roles of standing and transient eddies in the response of the Southern Ocean dynamics to changes in winds.

Moreover, when investigating the response of the Southern Ocean to the SAM, part of the discrepancy between model studies may be due to their different approaches of representing the SAM forcing itself. In model studies, these forcings generally fall into three categories: highly idealized perturbations (Oke and England 2004; Hallberg and Gnanadesikan 2006; Klinger and Cruz 2009, either a homogeneous increase or a poleward shift in winds), realistic perturbations (Lefebvre and Goose 2005; Farneti et al. 2010, both more intense and poleward shifted winds), and simulated wind anomalies within climate simulations (Farneti et al. 2010; Spence et al. 2010). Hence, there remains a need to document the effect of such differences in wind forcings onto Southern Ocean dynamics, and in particular the effect of the spatial distribution of wind anomalies.

Here we assess the dynamical response of the Southern Ocean to the SAM focusing on (i) how eddies affect this response and (ii) the extent to which changes in the spatial pattern of the SAM matters. To do so we run simulations with a regional model of the Southern Ocean at two eddy-permitting resolutions, independently varying Southern Hemisphere wind intensity and patterns, consistent with a positive phase of the SAM. Analysis focuses on the corresponding changes in ACC transport and Southern Ocean MOC.

2. Methods

a. Ocean model

Our study uses the NEMO system (*Nucleus for European Modeling of the Ocean*, Madec (2008)) which couples the hydrostatic, primitive equation ocean model OPA (Madec et al. 1998) with the Louvain-la-Neuve sea-ice model LIM (Fichefet and Maqueda 1997). For atmospheric forcing, we use the DRAKKAR Forcing Set 3 (DFS3), a combined product using air temperature, humidity, and 10-m winds from ERA-40 (until year 2001) then ECMWF (*European Center for Medium-Range Weather Forecasts*, from 2002 to 2004) along with precipitation and radiation variables from satellite observations (Brodeau et al. 2010).

Simulations performed in this study are consistent with the hierarchy of models developed during the DRAKKAR project (Drakkar Group 2007). That is, we use a regional extraction from the global grid, designated *ORCA*, which includes all ocean south of 30°S and is designated *PERIANT*. This regional model is used here at two different nominal horizontal resolutions of 0.5° (PERIANT05) and 0.25° (PERIANT025). Both have 46 vertical levels with refined spacing at the surface (6 m) and increasing with depth to 250 m in the deepest level. Table 1 shows that our model resolutions are comparable to the resolutions used by the other high-resolution model configurations that have been used elsewhere for similar studies on the Southern Ocean sensitivity to winds. To facilitate comparison between simulations at 0.5° and 0.25° horizontal resolutions, we avoided using any eddy induced advection parameterization, such as that of Gent and McWilliams (1990). Vertical mixing is represented using a TKE (Turbulent Kinetic Energy) scheme and a background vertical mixing coefficient of 10^{-5} m^2 s^{-1} (Madec 2008) with enhanced mixing in case of static in-

stability.

In both 0.5° and 0.25° regional simulations, the northern boundary at 30°S is open and forced under radiation conditions (Treguier et al. 2001) with the output of the corresponding DRAKKAR global simulations ORCA05-G70 and ORCA025-G70, respectively (Barnier et al. 2006; Biastoch et al. 2008). Those global simulations have been shown to be in reasonable agreement with the observations (e.g. Lombard et al. 2009) in particular in the Southern Ocean (e.g. Treguier et al. 2007).

For all simulations, the ocean starts at rest and temperature and salinity are initialised with the National Oceanographic Data Center World Ocean Atlas 1998 (Levitus et al. 1998). Simulations were limited to the period 1980–2004 to avoid potentially erroneous interseasonal variability of Southern Ocean winds in the pre-satellite era (Bromwich and Fogt 2004). For analysis, we focus on the 1995–2004 period, after the circulation has stabilized following a 15-year spin-up (Fig. 3).

A common issue in z-coordinate ocean models is their inability to capture the descent of dense waters that become Antarctic Bottom Water (AABW, Winton et al. 1998; Lee et al. 2002). This artefact results in a slow downward trend in ACC transport in the global configurations ORCA05 and ORCA025 (Treguier et al. 2010), of which PERIANT05 and PERIANT025 are regional extractions. To overcome this common difficulty, some models relax deep-water temperature and salinity towards observations to maintain realistic values near the ocean bottom (e.g. Hallberg and Gnanadesikan 2006). In all our simulations, we apply a 3-D relaxation of AABW temperature and salinity towards climatological annual-mean values from Gouretski and Koltermann (2004) (see Appendix).

b. Synthetic forcing

For both horizontal resolutions, we carried out three sets of simulations: REFxxx refers to the set of control simulations where the reanalyzed atmospheric winds are unperturbed; WINDxxx refers to the set of simulations where the winds are increased homogeneously everywhere; and SAMxxx refers to simulations where winds are perturbed following the observed pattern of the SAM (poleward intensification). The suffix xxx designates other characteristics related to resolution and forcing intensity of individual simulations that will be detailed later. But first let us focus on how the synthetic forcing for the WINDxxx and SAMxxx simulations was constructed.

The ocean model forcing depends largely on the wind velocity at 10 m in the atmosphere, $\mathbf{U}(x, y, t)$. In the REFxxx simulations, the 10-m wind velocity is simply that from the atmospheric reanalysis ($\mathbf{U}_{ar}(x, y, t)$). In the WINDxxx simulations, the magnitude of $\mathbf{U}$ is permanently and homogeneously increased over the domain. In the SAMxxx simulations, a pattern $\mathbf{P}_{U_{ar}}$ which describes the spatial wind anomaly pattern of the SAM is added permanently. Hence the general formula for $\mathbf{U}$ may be written:

$$\mathbf{U}(x, y, t) = \alpha \mathbf{U}_{ar}(x, y, t) + \beta \mathbf{P}_{\mathbf{U}_{ar}}(x, y), \tag{1}$$

In equation (1), α and β are constants. Following Lefebvre and Goose (2005), $\mathbf{P}_{\mathbf{U}_{ar}}$ is the regression pattern of $\mathbf{U}_{ar}$ onto the SAM index, I_{SAM}, such that:

$$(\mathbf{U}_{ar}(x, y, t) - I_{SAM}(t) \cdot \mathbf{P}(x, y))^t (\mathbf{U}_{ar}(x, y, t) - I_{SAM}(t) \cdot \mathbf{P}(x, y)) \tag{2}$$

is minimized over the period 1980–2001 and over the model domain (south of 30°S). The index I_{SAM} is the 1980–2001 monthly SAM index built from products of the National Center

for Environmental Prediction (NCEP)[1].

Figure 1.a shows the zonal component of the regression pattern, $\mathbf{P}_{\mathbf{U}_{ar}}$, onto the SAM index. The pattern is extremely zonal with positive coefficients in southern regions near the ACC (around 60°S) and negative coefficients on the north side of the Southern Ocean. This overall structure corresponding to a positive phase of the SAM, is poleward intensification of zonal winds over the circumpolar ocean and weakening of zonal winds farther north, as described by many authors (e.g. Thompson et al. 2000; Hall and Visbeck 2002; Sen Gupta and England 2006).

The WINDxxx simulations use the forcing strategy of Hallberg and Gnanadesikan (2006), except that we modify wind velocity instead of the wind stress. Our model uses bulk formulae for ocean surface boundary conditions, implying that the wind velocity enters into calculations of wind stress, the momentum transfer coefficient, evaporation, sensible heat, and latent heat. Hence our modification of mechanical forcing (wind velocities) affects the thermodynamic forcing via surface fluxes. Additionally, bulk formulae provide a feedback from the ocean to the atmosphere via surface fluxes, even though we do not use a coupled ocean-atmosphere model. The SAMxxx simulations adopt the forcing strategy of Lefebvre and Goose (2005), except that we only built of series of synthetic forcings for wind whereas they also did the same for air temperature. We did not adjust air temperature. In conclusion, the two forcing strategies applied to a consistent set of simulations (WINDxxx and SAMxxx) represent a novel forcing approach that allows us to investigate the response of Southern Ocean dynamics to changes in the strength and pattern of the winds.

Details of the characteristics of these series of simulations are summarized in Table 2. At

---

[1]http://www.cpc.ncep.noaa.gov/products/precip/CWlink/daily_ao_index/aao/monthly.aao.index.b79.current.ascii

the 0.5° resolution, three simulations were made applying increasing wind intensity for each of the WINDxxx and SAMxxx series. At the 0.25° resolution, we made only two simulations to conserve computional resources. Thus we applied only the strongest wind anomaly to each type of perturbation. Thus the linearity of the response of the Southern Ocean response to changes in wind is only studied at the 0.5° resolution.

Figure 1.b shows the 1995–2004 average for zonal profiles of wind stress for the complete series of simulations at the 0.5° resolution. WIND05 simulations exhibit maxima always at the same latitude as the control (REF05), whereas maxima for the SAM05 simulations are shifted poleward by up to ∼3°, in agreement with observations and models (Visbeck 2009; Chen and Held 2007; Fyfe and Saenko 2006), thus simulating the poleward shift of zonal winds during positive phases of the SAM. In the WIND05 simulations, the wind velocity is increased by either 10, 20, or 30%. Thus the mean zonal wind stress is doubled (wind stress being a quadratic function of wind velocity) in the WIND05+++ simulation. In the SAM05 simulations, the mean zonal wind stress increase is lower, reaching at most 50% of that in the REF05 simulation.

c. Consistency of model simulations

The spatial pattern of Eddy Kinetic Energy (EKE) averaged over 1992–2002 in the REF05 and REF025 simulations are compared to the observations in Figure 2. Observational estimates of EKE come from TOPEX/Poseidon 1992–2002 data set (Ducet et al. 2000). In both models and observations, the most energetic regions are the latitudes of the ACC, the Agulhas Retroflection, the Brazil-Malvinas confluence, and the East Australian Current. At

9

both resolutions, simulated regional patterns generally agree well with those observed. Zonally integrated near-surface EKE averaged between 35°S and 65°S is 27 cm^2s^{-2} for REF05 and 69 cm^2s^{-2} for REF025, i.e. $\sim1/4$ and $\sim2/3$ of observed values, respectively. The reasonable match of REF025 with the observed pattern and magnitude of EKE helps confirm its adequacy for this study. Similar patterns, despite the expected lower magnitude of EKE in REF05, suggests that this intermediate-resolution version of the same model serves as an appropriate first step into the eddying regime. Using both models allows us to say more about the resolution that is needed to address how the SAM affects ocean dynamics.

Figure 3 shows the time series of the annual mass transport at Drake Passage in REF05 and REF025 regional simulations (PERIANT05 and PERIANT025), and in the corresponding ORCA05-G70 and ORCA025-G70 global simulations (ORCA05 and ORCA025). Global simulations were run for a longer period (1958–2004) than the regional simulations (1980–2004), but that cannot explain differences in the trends. After 8 years of spin-up, the trend flattens out in the regional simulations, whereas in the global simulations there is a downward trend even after 15 years of spin-up. The difference is due to the 3-D relaxation of AABW towards observed temperature and salinity (see Appendix) which was applied to regional simulations only. This relaxation maintains the deep meridional gradient of density in the Southern Ocean, stabilising ACC transport. Consequently, Drake Passage transport is more intense in the regional simulations than in the global simulations, by at least 10 Sv (1 Sv = 10^6 m^3s^{-1}). In REF05 and REF025, the transport at Drake Passage averaged over 1995–2004 is 142.6 Sv and 143.2 Sv, respectively. Observational estimates range from 110 Sv to 150 Sv (Whitworth 1983; Whitworth and Peterson 1985; Cunningham et al. 2003). Moreover, Drake Passage transport differs by only less than 1 Sv between REF05 and REF025.

10

In previous model studies, this ACC transport differs by tens of Sv depending in part on model resolution (e.g. Hallberg and Gnanadesikan 2006; Farneti et al. 2010).

Figure 4 shows the mean 1995–2004 salinity along the 115°E section of the Southern Ocean in the REF05 and REF025 simulations. Salty and weakly stratified waters are found at around 42°S at the subsurface corresponding to the Subantarctic Mode waters (SAMW). The low salinity layer (34.2-34.4 psu) which appears at intermediate depth is typical of Antarctic Intermediate waters (AAIW) and can be traced back from the surface. A salty tongue (more than 34.7 psu) is found at around 2000 m and corresponds to Circumpolar Deep Water (CDW) which flow southward and upwell near the Polar Front. The REF05 and REF025 simulations show few differences: fronts are more localized in REF025; SAMW is shifted northward in REF05 and is less salty than in REF025; AAIW extends deeper and is further south in REF05 than in REF025. Simulated structure and magnitude of salinity generally agree with observations (section I9 of the Southern Ocean WOCE Hydrographic Atlas, Orsi and Whitworth (2004)), although simulated AAIW and SAMW are slightly denser.

For detailed validation of the global simulations ORCA05-G70 and ORCA025-G70, see Barnier et al. (2006) and Biastoch et al. (2008).

3. Southern Ocean dynamical response to changes in wind pattern and intensity

a. Response of the ACC transport

1) Shift of the ACC mean position

The Polar Front (PF) and Subantarctic Front (SAF) are the two main fronts that compose the ACC, carrying between them up to 75% of the total ACC transport south of Australia (Rintoul and Sokolov 2001). Thus the position of those fronts provides a good indicator of ACC position. Here, we calculate the PF and SAF positions using a comparable method to that of Sallée et al. (2008), computing the surface dynamic height anomaly referenced to 1500 m. Following Sallée et al. (2008), the PF is defined by the 0.95-m contour and the SAF by the 1.20-m contour. Figure 2 shows the mean PF and SAF positions for the period 1995–2004 for REF05 and SAM05+++ simulations and their corresponding simulations at 0.25°. Also shown are the same front positions, but as given by Orsi et al. (1995)'s climatology (Fig. 2.e). In REF05 and REF025, the mean positions of the PF and SAF as well as their meanders are generally quite similar to those proposed by Orsi et al. (1995), although simulated fronts are shifted northward by 2-3° (see also Table 2). On average, the simulated ACC is wider than indicated by hydrographic observations from Orsi et al. (1995). The simulated ACC being wider than the observed appears due to the model's ability to resolve frontal meanders whereas those structures in observed climatologies are probably smoothed by averaging. Closer inspection of differences between the two resolutions reveals that the ACC in REF025 is much more spatially variable, with larger meanders and varying more in

12

width along its course, e.g., being narrower than REF05 in some places (at Drake Passage, on the Kerguelen Plateau) and wider in others (southeast Indian Ocean, south Australia and southeast Pacific). REF025 is able to better represent this variability because of its more energetic mesoscale activity and its better resolution of the bathymetry.

During positive phases of the SAM, fronts tend to shift poleward in the Atlantic and Indian basins but equatorward in the Pacific basin (Fig. 2). The response of the ACC mean position to positive SAM events is thus not zonally coherent. This may be due to the strong variations in the latitude of ACC fronts around the circumpolar belt, thus being exposed to different SAM-induced wind anomalies along their pathways, as Sallée et al. (2008) suggested. In addition, frontal variability driven by SAM positive events is stronger in SAM025+++ than in SAM05+++ simulation. Yet in many regions where major topographic highs extend well above the abyssal plain, such as over the South Atlantic mid-ocean ridge or Kerguelen Plateau, ACC fronts show no spatial variability. Besides, the WIND05+++ and WIND025+++ simulations both show similar large equatorward meanders downstream of the major topographic features as well as stronger responses than in the SAMxxx simulations (not shown).

Table 2 gives an estimation of the ACC mean position computed by averaging the PF and SAF mean positions over 1995–2004. Increasing winds narrow and strengthen the ACC. At a horizontal resolution of 0.5° positive SAM events shift the ACC mean position by less than 0.5°, either poleward or equatorward. Considering the 0.5° resolution though, this shift is insignificant and may be ascribed to the turbulent nature of the ACC. Conversely, results from SAM025+++ indicate a potentially significant poleward shift of 0.3° of the ACC mean position. However, to infer a systematic poleward shift, more simulations would be needed

at 0.25°, following the approach used with the 0.5° model. Besides, at both resolutions, the WINDxxx simulations show a significant and systematic equatorward shift of the ACC mean position of more than 1°.

In each experiment (WINDxxx or SAMxxx), the simulated frontal shifts are small. The response of the ACC mean position to the SAM positive forcing anomaly is less than 0.5°, despite the large increase in wind intensity and the poleward shift of zonal winds (3°) applied in our simulations. In particular, we find smaller poleward shifts in the ACC's mean position than previous estimates of 1.0°±0.9° (Fyfe and Saenko 2006) and 3.5° (Spence et al. 2010). Our results thus show that bathymetry may mainly determine the ACC pathway. However, downstream of major topographic highs, fronts become more sensitive to atmospheric forcing and thus more spatially variable (Sallée et al. 2008). In those regions, it is mainly the SAM-driven wind anomaly patterns that induce meridional shifts of fronts.

2) Acceleration of the ACC

Figure 5.a shows the time-averaged mass transport at Drake Passage for each simulation as a function of the average zonal wind stress across the whole domain. The set of simulations shows a large range of responses of the ACC transport to winds. However, the strongest response is a 12% increase in the ACC transport (from REF05 to SAM05+++).

To learn about the relative importance of the mechanisms controlling the SAMs influence on the ACC, we can compare the two sets of simulations, SAM05 and WIND05. In both sets, there is a strong linear relationship between the mean zonal wind stress and the mean ACC transport (the coefficient of determination $R^2 = 0.98$ for WIND05, and $R^2 = 0.93$ for

SAM05). But it is already known that larger zonal wind stress yields greater ACC transport (e.g. Marshall and Radko 2003). What is more telling is that the slope of the SAM05 series of simulations is far steeper than that for the WIND05 series. Thus SAM-driven anomalies in wind patterns are more efficient in accelerating the ACC than are homogeneous wind anomalies. This demonstrates that the spatial pattern of wind, and not only its magnitude, can play a major role in changing the ACC transport.

Likewise, comparing SAM05+++ to SAM025+++ demonstrates that by moving to the enhanced resolution, reduces the response of ACC transport to poleward intensified winds by nearly half, from +12% to +5%. Other modeling studies also indicate that the response of ACC transport to increased wind forcing is reduced as model resolution increases (Hallberg and Gnanadesikan 2006; Spence et al. 2010; Farneti et al. 2010). Yet the resolution increase between our WIND05+++ and WIND025+++ simulations produces the opposite tendency: increased resolution increases ACC transport response, i.e. for the case where there is a spatially homogenous increase in winds. Although the difference in ACC transport between WIND05+++ and WIND025+++ is small and further experiments are required to confirm the systematic nature of this result, this finding does provide a counter-example to the necessary reduction in a model's ACC transport sensitivity with increasing resolution.

b. *Response of the meridional overturning circulation*

It is appropriate to consider the MOC in potential density, rather than in depth space, to obtain a relevant representation of the transport of water masses (e.g. Treguier et al. 2007). Following the lead of Döös and Webb (1994), we analyze results in terms of the total

meridional overturning streamfunction, Ψ_{tot}, expressed as:

$$\Psi_{tot}(y, \sigma_2) = \overline{\oint \int_{-H}^{\tilde{z}(x,y,\sigma_2)} v\, d\tilde{z}'\, dx,} \tag{3}$$

where σ_2 is the 2000-m depth referenced potential density, H is the spatially varying ocean bottom depth, $\tilde{z}$ is the depth of the σ_2 isopycnal, v is the meridional velocity, and the overbar denotes a temporal average at constant depth. Thus for some variable ξ over a period τ, $\overline{\xi} = \int_0^\tau \xi dt/\tau$. Then, the transient eddy-induced circulation Ψ^*, i.e. that due to deviations from the temporal mean, is defined following Treguier et al. (2007) as:

$$\begin{cases} \overline{\Psi}(y, \sigma_2) = \oint \int_{-H}^{\overline{\tilde{z}(x,y,\sigma_2)}} \overline{v} d\overline{\tilde{z}'} dx, \\ \\ \Psi^* = \Psi_{tot} - \overline{\Psi} \end{cases} \tag{4}$$

where $\overline{\Psi}$ is the mean Eulerian circulation computed from the time-mean velocity and the time-mean potential density field.

Figure 6 shows the resulting total meridional overturning computed from 5-day-averaged output from the simulations, and its mean Eulerian and transient-eddy contributions for each simulation during the 1995–2004 period. For the total meridional overturning (Fig. 6, left column), the strong uppermost blue cell extending from roughly 40°S corresponds to the wind-driven *subtropical cell*. That cell transports light waters southward, and as they cool they are transformed into SAMW. The red cell which extends until 57°S corresponds to the *subpolar cell* where North Atlantic Deep Waters (NADW) coming from the north are brought to the surface at 57°S by Ekman pumping, transformed into AAIW by surface fluxes, and then flow back to the north. Below that is the blue cell that corresponds to the *deep cell* where CDW upwell farther south, are transformed into AABW, and then move downward and northward along the slope of the Antarctic continent. Finally, the upper blue

16

cell which extends from 45°S to 65°S is the expression of waters cooling, and thus becoming denser, as they move southward while flowing along the ACC. This upper cell is not apparent when the MOC is computed along streamlines rather than latitude lines (Treguier et al. 2007). However, it does constitute a genuine overturning in density space. The mean Eulerian overturning (Fig.6, middle column) shows the same general structure as the total overturning, but it is partly compensated by the transient-eddy overturning (Fig.6, right column) as detailed in equation (4).

The subtropical, subpolar, and deep cells of the total overturning are similar in REF05 and REF025 simulations, each cell transporting up to ~15 Sv, ~8 Sv, and ~10 Sv, respectively. While intensities of both subtropical and subpolar cells of the mean Eulerian overturning do not change while increasing resolution (~-15 Sv and ~12 Sv), the upper cell linked to the surface ACC pathway shows an intensification of up to ~-5 Sv in REF025.

1) MODIFICATION OF THE MOC DENSITY STRUCTURE

In the 0.25° model, the SAM-induced poleward shift in winds (the move from REF025 to SAM025+++) results in a ~4° southward shift in the southernmost extent of the subpolar cell of the total overturning (Fig. 6). That southward shift is similar to the ~3° shift found by Farneti et al. (2010) with their CM2.4 model. Yet there is no such shift in our 0.5° model, i.e., between REF05 to SAM05+++. This southward shift is related to the significant, albeit weak, poleward shift in the ACC mean position in the SAM025+++ simulation (see Section 3.1). Additionally, the subpolar cell transforms deep into intermediate waters in different ways in the different sets of simulations. The subsequent intermediate waters are

17

denser in the SAMxxx simulations ($\sim$35.9 kg m^{-3}) than in the REFxxx simulations ($\sim$35.7 kg m^{-3}). Conversely, much lighter intermediate waters are found in the WINDxxx simulations ($\sim$35.4 kg m^{-3}). This last result is consistent with what Hallberg and Gnanadesikan (2006) found in their study. Thus the overlying subptropical cell transforms denser waters in the SAMxxx simulations ($\sim$35.8 kg m^{-3}) than in the REFxxx and WINDxxx simulations ($\sim$35.5 kg m^{-3} and $\sim$35.2 kg m^{-3}, respectively). This water mass densification consequent to a poleward shift of zonal winds may be related to a cooling of SAMW as suggested by Oke and England (2004).

The density of newly formed water masses is affected by any anomalous intensification of zonal winds over the ACC latitudes, which leads to a change in wind curl and thus a change in the location of the Ekman divergence. Hence deep waters coming from the north upwell at higher latitudes where they interact with a colder atmosphere, release more heat, and are transformed into denser water masses. However, when the wind is increased everywhere homogeneously over the Southern Ocean (our WINDxxx simulations), the ACC's fronts shift equatorward, forcing downwelling of intermediate waters to occur at more northern latitudes and along lighter isopycnal surfaces.

Therefore, SAM positive events can indeed imply significant changes in water mass properties and in turn, affect their rate of formation, as shown by previous studies (Oke and England 2004; Sen Gupta and England 2006; Hallberg and Gnanadesikan 2006). However, our results also point out that the MOC density structure responds in a very different way to homogeneous wind anomalies than to SAM-induced wind anomalies.

18

2) Intensification of the subpolar MOC

The increase in the Southern Ocean carbon sink with rising atmospheric CO_2 may be diminished by the SAM-induced intensification of the MOC, which enhances upwelling of DIC-rich deep waters to the surface (Lenton and Matear 2007; Lovenduski et al. 2007, 2008). As upwelling of deep water is effected by the subpolar cell; we focus on its response to wind anomalies.

To estimate subpolar MOC intensity, we computed the maximum of Ψ_{tot} in the subpolar cell between 40°S and 55°S. Results are shown in Figure 5.b for each simulation as a function of the mean zonal wind stress over the model domain. Simulated responses of the subpolar MOC to winds vary greatly, with the strongest response being a 153% increase in the subpolar MOC in the WIND05+++ simulation. Our results exhibit much greater sensitivity of the subpolar MOC to changes in winds relative to previous modeling studies (Hallberg and Gnanadesikan 2006; Farneti et al. 2010).

Comparing results in simulations at the 0.5° resolution indicates nearly linear relationships within each set, but different sensitivities between them. Linear fits between mean subpolar MOC intensity versus mean zonal wind stress result in a coefficient of determination $R^2 > 0.99$ for the WIND05 simulations and $R^2 = 0.91$ for the SAM05 runs. Thus, wind largely determines MOC intensity, as discussed previously (Gnanadesikan and Hallberg 2000; Karsten et al. 2002). Yet the slope for the WIND05 series is steeper than that for the SAM05 series, implying that a spatially homogeneous increase in wind anomalies intensifies the subpolar MOC more than does the SAM-driven change in their spatial pattern. Indeed, in the WIND05 series of simulations, wind stress is increased over a greater range of lati-

tudes. Thus, intensification in Ekman pumping both north and south of the ACC is spread out over a wider range of latitudes in the WIND05 simulations, perhaps leading to a stronger change in the subpolar MOC.

In contrast, the effect of resolution on the subpolar MOC is mixed between the two types of wind perturbations (Fig. 5b). Better resolving eddies attenuates the response of the subpolar MOC to a spatially homogeneous increase in winds (WIND025+++ vs. WIND05+++) but enhances its response to a SAM-induced pattern change in winds (SAM025+++ vs. SAM05+++). Enhanced mesoscale activity (better resolution) is expected to attenuate the response of the subpolar MOC to increased wind stress, as reported by Hallberg and Gnanadesikan (2006) and Farneti et al. (2010). They argue that such an attenuation occurs because enhanced resolution allows transient eddy fluxes to better compensate for the increased Ekman transport in the MOC. Yet in our SAM025+++ simulation, the role of transient eddies in the meridional overturning becomes almost negligible (Fig. 6, bottom-right panel). This reduction of the transient eddy meridional overturning with resolution occurs despite an increase in EKE and reduced ACC transport, both of which indicating a more active transient eddy field. Thus some process besides meridional fluxes from transient eddies must compensate for the large increase in zonal Ekman transport, as discussed below.

4. Discussion

As illustrated in equation (4), the total circulation Ψ_{tot} can be decomposed into a mean Eulerian circulation $\overline{\Psi}$ and a transient eddy-induced circulation Ψ^*. The $\overline{\Psi}$ term represents the temporal mean flow. Thus it includes both the contribution of the zonally averaged flow

(mainly the Ekman transport) and the meridional excursions from the zonal mean (standing eddies, Ivchenko et al. (1996)). In the same way that the MOC can be separated into its temporal mean and transient eddy (perturbation) components, so can the temporal mean be separated into its zonally averaged and standing eddy components (see Lee and Coward (2003) for a similar decomposition):

$$
\begin{cases}
\overline{\Psi} = <\overline{\Psi}> + \overline{\Psi}_{SE} \\
<\overline{\Psi}> (y, \sigma_2) = \oint \int_{-H}^{<\overline{\tilde{z}(y,\sigma_2)}>} <\overline{v}> d <\overline{\tilde{z}'}> dx,
\end{cases}
\tag{5}
$$

where the angular brackets denote a zonal average at constant depth. A zonal average for a function ξ and latitude circle of length L is thus $<\xi> = \oint \xi dx / L$. The streamfunction $<\overline{\Psi}>$ is effectively the mean Eulerian MOC zonally averaged at constant depth and projected onto the zonally averaged density. At latitudes of Drake Passage, $<\overline{\Psi}>$ essentially corresponds to a northward Ekman transport on shallow layers and a southward geostrophic transport on layers whose mean depth is below the Drake Passage. The streamfunction $\overline{\Psi}_{SE}$ accounts for the standing eddy overturning circulation. Thus, the total circulation can be defined in terms of three main contributions,

$$
\Psi_{tot} = <\overline{\Psi}> + \overline{\Psi}_{SE} + \Psi^*,
\tag{6}
$$

i.e. from the zonal-average mean Eulerian flow, standing eddies, and transient eddies.

Figure 7 shows $<\overline{\Psi}>$ and $\overline{\Psi}_{SE}$ for SAM05+++ and SAM025+++, averaged over 1995–2004. In both simulations, $<\overline{\Psi}>$ is partly compensated by $\overline{\Psi}_{SE}$. At the higher resolution, the standing eddy-driven circulation is reinforced. As in Section 2, for an index of the MOC intensity for each $<\overline{\Psi}>$ and $\overline{\Psi}_{SE}$, we compute the maximum value between 40°S and 55°S. Enhancing resolution (moving from SAM05+++ to SAM025+++) enhances

the compensation of zonal-average mean Eulerian flow ($< \overline{\Psi} >$) achieved by standing eddy flow ($\overline{\Psi_{SE}}$) by more than 10% (see also Fig. 7). Therefore, higher resolution allows for meridional transport from standing eddies to better compensate for enhanced Ekman transport from intensified winds. Similar results are found by comparing the WIND05+++ and WIND025+++ simulations (not shown).

Although higher resolution in our models enhances meridional fluxes from standing eddies, it reduces meridional fluxes from transient eddies (Fig.6). The majority of the overturning circulation is thus a balance of Ekman transport and the time-mean geostrophic flow. Although the dominance of standing eddies in the eddy compensation of the enhanced wind-driven overturning has not been pointed out in the literature (to our knowledge), this result does find some support in previous studies. Farneti et al. (2010), for instance, subjected two fine-resolution models to present day and SAM-like forcing anomalies (CTL and SHW3X simulations). They found a transient eddy driven overturning response of only 2-3 Sv (their Fig.10), indicating that the standing eddy driven overturning might balance almost all the wind-driven overturning. Moreover, using an eddy-permitting global ocean model, Lee and Coward (2003) highlighted the role of standing eddies in cancelling the wind-driven circulation.

Enhanced resolution alters standing eddy meridional fluxes because it allows for (1) enhanced deviations from the zonal mean of velocity ($v- < v >$) and (2) enhanced deviations in the zonal mean of isopycnal thickness ($h- < h >$, where $h = \dfrac{d\tilde{z}}{d\sigma_2}$), i.e., stratification. Higher resolution implies finer topography, thus better resolving standing eddies (see Fig.2) and allowing them to be more vigorous (changing $v- < v >$). Enhanced resolution may also cause large-scale changes in stratification, perhaps in part from transient eddies.

Figure 8 summarises the results on the intensity in ACC transport and MOC subpolar cell responses to a wind modification at the two eddy-permitting resolutions. The simulated response of Southern Ocean dynamics to a wind anomaly is not straightforward. In particular, this response depends on both numerical resolution and spatial pattern of wind anomalies. This response also dramatically differs when considering either ACC or MOC responses. Hence, our results show that there is no simple link between the two. Moreover, the MOC appears to be more sensitive to wind changes than the ACC. This result is in agreement with the study of Meredith et al. (2011) which used theoretical arguments to suggest that in an eddy-saturated Southern Ocean (that is with the ACC being only weakly sensitive to wind stress change), the response of the Southern Ocean overturning to wind stress changes is likely to be substantial. Indeed, dynamical and thermodynamical processes may not set at the same order the respective balances of the MOC and ACC transports.

5. Conclusion

A regional ocean-sea ice model of the Southern Ocean configured at two eddy-permitting resolutions (0.5° and 0.25°) was forced by atmospheric reanalysis products during 1980–2004 and perturbed to study how SAM pattern and intensity affect the ACC and MOC.

During positive phases of the SAM, ACC transport increases by ∼10% and is weakly shifted poleward by less than 0.5° as a result of a stronger wind stress and modified wind curl. The increased wind stress intensifies the subpolar MOC, confirming that the overturning circulation is set at first order by the wind-driven circulation. There are also substantial

23

changes in the MOC's density structure: the subpolar cell shifts poleward by $\sim 4°$ while the overturning draws on denser intermediate waters.

As resolution increases, standing eddy fluxes more efficiently balance the Ekman flow; conversely, meridional transient eddy fluxes are not enhanced with increasing winds and resolution. Indeed, only standing eddies compensate meridional fluxes from the wind-driven circulation when the spatial pattern of the winds associated with the SAM is applied to the 0.25° model (simulation SAM025+++). Thus standing eddies play a crucial role in the meridional overturning of the Southern Ocean.

In a recent study by Böning et al. (2008), an apparent small sensitivity of the ACC to changes in the Southern Hemisphere winds is observed. Those authors use this result to argue that the MOC may not be highly sensitive to wind changes either. Our results demonstrate that the ACC and MOC can exhibit very different sensitivities to wind perturbations. Hence, it is not straightforward to infer a change in the MOC from a change in ACC transport.

Finally, modifying the pattern of wind anomalies leads to opposing responses of the ACC and MOC. SAM-driven wind anomalies are found to be far more efficient at accelerating the ACC than homogeneous wind anomalies. Thus simulations that aim to simulate the response of the Southern Ocean to the SAM should account not only for the increase in winds but also the change in the pattern (driven by the contraction of the polar vortex). Moreover, our result implies that differences between wind pattern tendencies, as resolved by climate models, may induce significant discrepancies in the projected Southern Ocean dynamics.

APPENDIX

3-D thermohaline restoring of AABW

Thermohaline properties of Antarctic Bottom Waters (AABW) are restored towards the observed climatology of Gouretski and Koltermann (2004) as described below.

Following Orsi et al. (1999), in the Southern Ocean, AABW are the water mass having $\sigma_2 > 37.16$ kg m^{-3}, where σ_2 is the potential density referenced at 2000 m. With this density criterion, we constructed a mask (M) of the domain as follows:

$$M(x, y, z) = g(\sigma_2(x, y, z)) \cdot h(z) \tag{A1}$$

$$with \begin{cases} g(\sigma_2(x, y, z)) = \frac{1}{2}\left[\frac{tanh[(\sigma_2(x,y,z) - \sigma_{ref}]}{\alpha} + 1\right] \\ h(z) = \frac{1}{2}\left[\frac{tanh[(z - z_{ref}]}{\beta} + 1\right] \end{cases} \tag{A2}$$

where σ_2 is computed from the annual climatology of Gouretski and Koltermann (2004), $\sigma_{ref} = 37.16$ kg m^{-3}, $\alpha = 0.025$ kg m^{-3}, $z_{ref} = 1000$ m, and $\beta = 100$ m. Thus M has values that range from 0 to 1.

Although the NODC World Ocean Atlas 1998 (WOA1998) monthly climatology was used to initialize model temperature and salinity fields, we used the annual climatology of Gouretski and Koltermann (2004) to build this deep restoring mask and apply the restoring in our simulations, because it was computed with an interpolation method that avoids creating spurious water masses as in WOA1998 (Levitus et al. 1998).

Throughout each simulation, model temperature and salinity are restored to the annual

climatology of Gouretski and Koltermann (2004) as follows:

$$\begin{cases} \partial_t \Theta(t,x,y,z) = ... + \frac{M(x,y,z)}{\tau}(\Theta_{clim}(x,y,z) - \Theta(t,x,y,z)) \\ \partial_t S(x,y,z) = ... + \frac{M(x,y,z)}{\tau}(S_{clim}(x,y,z) - S(t,x,y,z)) \end{cases} \quad (A3)$$

where Θ and S are potential temperature and salinity computed by the model, respectively,

Θ_{clim} and S_{clim} are potential temperature and salinity from the annual climatology of Gouret-

ski and Koltermann (2004), and τ is the restoring time scale.

Figure 9 shows the ratio of water depth restored with a time scale of less than ten years in

our simulations, i.e., with a total restoring coefficient $\frac{M(x,y,z)}{\tau} > 3.17 \ 10^{-9} \ \mathrm{s}^{-1}$, corresponding

to a mask coefficient $M(x,y,z) > 0.2$ and a restoring time scale $\tau = 2$ years. The constraint

on the model AABW is strongest around the Antarctic mainland and gradually weakens to

the north. This gradient is due to very dense water masses which forming on the Antarctic

ice shelves that then spread northward along the continental slope. Yet restoring is weak in

the latitude band of the ACC.

The efficiency of our restoring method was tested in regional simulations of the Southern

Ocean over 1991–2000 using the same modelling system (Section 2 details the model and

configuration used). With this model we made sensitivity tests to refine the potential den-

sity criterion σ_{ref} (determining the volume of water restored) and the restoring time scale

τ. All of theses tests required shorter spin-ups than did the reference simulation; the ACC

transport stabilized after only 8 years (see Fig.3). After the spin-up, there was no longer a

trend in ACC transport as opposed to the non-restored simulation. Interannual variability

of ACC transport was not affected by restoring of bottom-water temperature and salinity.

Yet the larger the restoring constraint, the greater was the ACC transport. Thus the σ_{ref}

and τ criteria were chosen to yield reasonable ACC transport intensity while maintaining

27

values that provided only a weak constraint on the model. A similar approach was also used by Hallberg and Gnanadesikan (2006) who applied weak sponges around the Antarctic ice shelves to ensure the formation of AABW. They also noticed that this restoring influenced the net ACC transport.

REFERENCES

Barnier, B., et al., 2006: Impact of partial steps and momentum advection schemes in a global ocean circulation model at eddy permitting resolution. *Oc. Dynam.*, **56**, 543–567.

Biastoch, A., C. Böning, J. Getzlaff, J. Molines, and G. Madec, 2008: Causes of Interannual-Decadal Variability in the Meridional Overturning Circulation of the Midlatitude North Atlantic Ocean. *J. Climate*, **21**, 6599–6615.

Böning, C., A. Dispert, M. Visbeck, S. Rintoul, and F. Schwarzkopf, 2008: The response of the Antarctic Circumpolar Current to recent climate change. *Nat. Geosci.*, **1**, 864–869.

Brodeau, L., B. Barnier, T. Penduff, A.-M. Treguier, S. Gulev, and T. J. McDougall, 2010: An ERA-40 based atmospheric forcing for global ocean circulation models. *Oc. Modell.*, **31**, 88–104.

Bromwich, D. H. and R. L. Fogt, 2004: Strong trends in the Skill of the ERA-40 and NCEP-NCAR Reanalyses in the High and Midlatitudes of the Southern Hemisphere, 1958-2001. *J. Climate*, **17**, 4603–4619.

Cai, W. and P. H. Whetton, 2003: The Response of the Antarctic Oscillation to Increasing and Stabilized Atmospheric CO_2. *J. Climate*, **16**, 1525–1538.

Chen, G. and I. M. Held, 2007: Phase speed spectra and the recent poleward shift of Southern Hemisphere surface westerlies. *Geophys. Res. Letters*, **34**, L21 805.

Cunningham, S. A., S. G. Alderson, B. A. King, and M. A. Brandon, 2003: Transport and variability of the Antarctic Circumpolar Current in Drake Passage. *J. Geophys. Res.*, **108**, NO. C5, 8084.

Döös, K. and D. J. Webb, 1994: The Deacon Cell and the Other Meridional Cells of the Southern Ocean. *J. Phys. Oceanogr.*, **24**, 429–442.

Drakkar Group, 2007: Eddy-permitting Ocean Circulation Hindcasts of past decades. *CLIVAR Exchanges*, **12**, 8–10.

Ducet, N., P.-Y. L. Traon, and G. Reverdin, 2000: Global high resolution mapping of ocean circulation from Topex/Poseidon and ERS-1 and -2. *J. Geophys. Res.*, **105(C8)**, 19 477–19 498.

Farneti, R., T. L. Delworth, A. J. Rosati, S. M. Griffies, and F. Zeng, 2010: The role of mesoscale eddies in the rectification of the southern ocean response to climate change. *J. Phys. Oceanogr.*, **40**, 1539–1557.

Fichefet, T. and M. A. M. Maqueda, 1997: Sensitivity of a global sea ice model to the treatment of ice thermodynamics and dynamics. *J. Geophys. Res.*, **102**, 12,609–12,646.

Fyfe, J. C. and O. A. Saenko, 2006: Simulated changes in the extratropical Southern Hemisphere winds and currents. *Geophys. Res. Letters*, **33**, L06 701.

Gent, P. R. and J. C. McWilliams, 1990: Isopycnal Mixing in Ocean Circulation Models. *J. Phys. Oceanogr.*, **20**, 150–155.

Gnanadesikan, A. and R. W. Hallberg, 2000: On the Relationship of the Circumpolar

Current to Southern Hemisphere Winds in Coarse-Resolution Ocean Models. *J. Phys. Oceanogr.*, **30**, 2013–2034.

Gouretski, V. and K. Koltermann, 2004: Woce global hydrographic climatology, a technical report. *Berichte des BSH*, **35**.

Hall, A. and M. Visbeck, 2002: Synchronous Variability in the Southern Hemisphere Atmosphere, Sea Ice, and Ocean Resulting from the Annular Mode. *J. Climate*, **15**, 3043–3057.

Hallberg, R. and A. Gnanadesikan, 2006: The Role of Eddies in Determining the Structure and Response of the Wind-Driven Southern Hemisphere Overturning: Results from the Modeling Eddies in the Southern Ocean (MESO) Project. *J. Phys. Oceanogr.*, **36**, 2232–2252.

Ivchenko, V., K. Richards, and D. Stevens, 1996: The Dynamics of the Antarctic Circumpolar Current. *J. Phys. Oceanogr.*, **26**, 753–774.

Karsten, R., H. Jones, and J. Marshall, 2002: The Role of Eddy Transfer in Setting the Stratification and Transport of a Circumpolar Current. *J. Phys. Oceanogr.*, **32**, 39–54.

Klinger, B. A. and C. Cruz, 2009: Decadal response of global circulation to southern ocean zonal wind stress perturbation. *J. Phys. Oceanogr.*, **39**, 1888–1904.

Le Quéré, C., et al., 2007: Saturation of the southern ocean CO_2 sink due to recent climate change. *Science*, **316**, 1735–1738.

Lee, M.-M. and A. C. Coward, 2003: Eddy mass transport for the southern ocean in an eddy-permitting global ocean model. *Oc. Modell.*, **5**, 249–266.

Lee, M.-M., A. C. Coward, and A. J. G. Nurser, 2002: Spurious diapycnal mixing of the deep waters in an eddy-permitting global ocean model. *J. Phys. Oceanogr.*, **32**, 1522–1535.

Lefebvre, W. and H. Goose, 2005: Influence of the Southern Annular Mode on the sea ice-ocean system: the role of the thermal and mechanical forcing. *Oc. Science*, **1**, 145–157.

Lenton, A. and R. J. Matear, 2007: Role of the Southern Annular Mode (SAM) in Southern Ocean CO_2 uptake. *Global Biogeochem. Cycles*, **21**.

Levitus, S., et al., 1998: World ocean database 1998. *NOAA Atlas NESDID 18, US Governement Printing Office, Whashingthon, DC*, **40**, 150.

Lombard, A., G. Garric, and T. Penduff, 2009: Regional patterns of observed sea level change: Insights from a 1/4°global ocean/sea-ice hindcast. *Oc. Dynamics*, **59(3)**, 433–449.

Lovenduski, N., N. Gruber, and S. Doney, 2008: Toward a mechanistic understanding of the decadal trends in the Southern Ocean carbon sink. *Global Biogeochem. Cycles*, **22**, GB3016.

Lovenduski, N., N. Gruber, S. Doney, and I. Lima, 2007: Enhanced CO2 outgassing in the Southern Ocean from a positive phase of the Southern Annular Mode. *Global Biogeochem. Cycles*, **21**, GB2026.

Madec, G., 2008: Nemo ocean engine. *Note du Pôle de modelisation, Institut Pierre-Simon Laplace (IPSL), France*, **27**, ISSN 1288–1619.

Madec, G., P. Delecluse, M. Imbard, and C. Lévy, 1998: OPA8.1 Ocean General Circulation

Model reference manual. *Note du Pôle de modelisation, Institut Pierre-Simon Laplace (IPSL), France*, 91 pp.

Marshall, G. J., 2003: Trends in the Southern Annular Mode from Observations and Re-analyses. *J. Climate*, **16**, 4134–4143.

Marshall, G. J., P. A. Stott, J. Turner, W. M. Connolley, J. C. King, and T. A. Lachlan-Cope, 2004: Causes of exceptional atmospheric circulation changes in the Southern Hemisphere. *Geophys. Res. Lett.*, **31**, L14 205.

Marshall, J. and T. Radko, 2003: Residual-mean solutions for the antarctic circumpolar current and its associated overturning circulation. *J. Phys. Oceanogr.*, **33**, 2341–2354.

Meredith, M. P., A. C. N. Garabato, A. M. C. Hogg, and R. Farneti, 2011: Sensitivity of the overturning circulation in the southern ocean to decadal changes in wind forcing. *Journal of Climate*, **in press**.

Meredith, M. P. and A. M. Hogg, 2006: Circumpolar response of Southern Ocean eddy actvity to a change in the Southern Annular Mode. *Geophys. Res. Lett.*, **33**, L16 608.

Meredith, M. P., P. L. Woodworth, C. W. Hughes, and V. Stepanov, 2004: Changes in the ocean transport through drake passage during the 1980s and 1990s, forced by changes in the Southern Annular Mode. *Geophysical Research Letters*, **31**, L21 305.

Metzl, N., B. Tilbrook, and A. Poisson, 1999: The annual fCO_2 cycle and the air-sea CO_2 flux in the sub-Antarctic Ocean. *Tellus*, **51**, 849–861.

Naveira Garabato, A. C., L. Jullion, D. P. Stevens, K. J. Heywood, and B. A. King, 2009:

Variability of Subantarctic Mode Water and Antarctic Intermediate Water in the Drake Passage during the Late-Twentieth and Early-Twenty-First Centuries. *Journal of Climate*, **22**, 3661–3688.

Oke, P. R. and M. R. England, 2004: Oceanic Response to Changes in the Latitude of the Southern Hemisphere Subpolar Westerly Winds. *J. Climate*, **17**, 1040–1054.

Orsi, A., T. W. III, and J. W. Nowlin, 1995: On the meridional extent and fronts of the Antarctic Circumpolar Current. *Deep Sea Res., Part II*, **42**, 641–673.

Orsi, A., G. Johnson, and J. Bullister, 1999: Circulation, mixing, and roduction of Antarctic Bottom Water. *Progress in Oceanography*, **43**, 55–109.

Orsi, A. and T. Whitworth, 2004: Hydrographic Atlas of the World Ocean Circulation Experiment (WOCE). Volume 1 : Southern Ocean. *International WOCE Project Office, Southampton, U.K.*

Rintoul, S. and S. Sokolov, 2001: Baroclinic transport variability of the Antarctic Circumpolar Current south of Australia (WOCE repeat section SR3). *J. Geophys. Res.*, **106**, 2795–2814.

Sallée, J.-B., K. Speer, and R. Morrow, 2008: Response of the Antarctic Circumpolar Current to Atmospheric Variability. *J. Climate*, **21**, 3020–3039.

Sen Gupta, A. and M. H. England, 2006: Coupled Ocean-Atmosphere-Ice Response to Variations in the Southern Annular Mode. *J. Climate*, **19**, 4457–4486.

Spence, P., J. C. Fyfe, A. Montenegro, and A. J. Weaver, 2010: Southern Ocean response

to strenghening winds in an eddy-permitting global climate model. *J. Climate*, **23**, 5332–5343.

Thompson, D. W. J. and S. Solomon, 2002: Interpretation of recent Southern Hemisphere climate change. *Science*, **296**, 895–899.

Thompson, D. W. J., J. M. Wallace, and G. C. Hegerl, 2000: Annular Modes in the Extratropical Circulation. Part II: Trends. *J. Climate*, **13**, 1018–1036.

Treguier, A., J. L. Sommer, J. Molines, and B. D. Cuevas, 2010: Response of the Southern Ocean to the Southern Annular Mode: interannual variability and multidecadal trend. *J. Phys. Oceanogr.*, **40**, 1659–1668.

Treguier, A.-M., B. Barnier, A. D. Miranda, J. Molines, N. Grima, M. Imbard, G. Madec, and C. Messager, 2001: An eddy-permitting model of the Atlantic circulation: Evaluating open boundary conditions. *J. Geophys. Res. - Oceans*, **106**, 22 115–22 129.

Treguier, A.-M., M. H. England, S. R. Rintoul, G. Madec, J. Le Sommer, and J.-M. Molines, 2007: Southern Ocean overturning across streamlines in an eddying simulation of the Antarctic Circumpolar Current. *Oc. Science*, **3**, 491–507.

Visbeck, M., 2009: A Station-Based Southern Annular Mode Index from 1884 to 2005. *J. Climate*, **22**, 940–950.

Whitworth, T., 1983: Monitoring the Transport of the Antarctic Circumpolar Current at Drake Passage. *J. Phys. Oceanogr.*, **13**, 2045–2057.

Whitworth, T. and R. Peterson, 1985: Volume transport of the Antarctic Circumpolar Current from bottom pressure measurements. *J. Phys. Oceanogr.*, **15**, 810–816.

Winton, M., R. Hallberg, and A. Gnanadesikan, 1998: Simulation of Density-Driven Frictional Downslope Flow in Z-Coordinate Ocean Models. *J. Phys. Oceanogr.*, **28**, 2163–2174.

Yang, X., R. Huang, J. Wang, and D. Wang, 2008: Delayed baroclinic response of the Antarctic circumpolar current to surface wind stress. *Science in Chine Series D: Earth Sciences*, **51**, 1036–1043.

List of Figures

FIG. 1. (a) Regression pattern (m s^{-1} std^{-1}(I$_{SAM}$); I$_{SAM}$ being the SAM index) of 1980–2001 monthly averaged ERA-40 zonal winds onto the NCEP 1980–2001 monthly SAM index (contours are given every 0.2 units; solid lines indicate positive values and dashed lines indicate negative values). (b) Mean zonal wind stress over 1994–2005 (N m^{-2}) for the 0.5° series of simulations: REF05 (solid), WIND05+, WIND05++, and WIND05+++ (dashed), and SAM05+, SAM05++, and SAM05+++ (dotted).
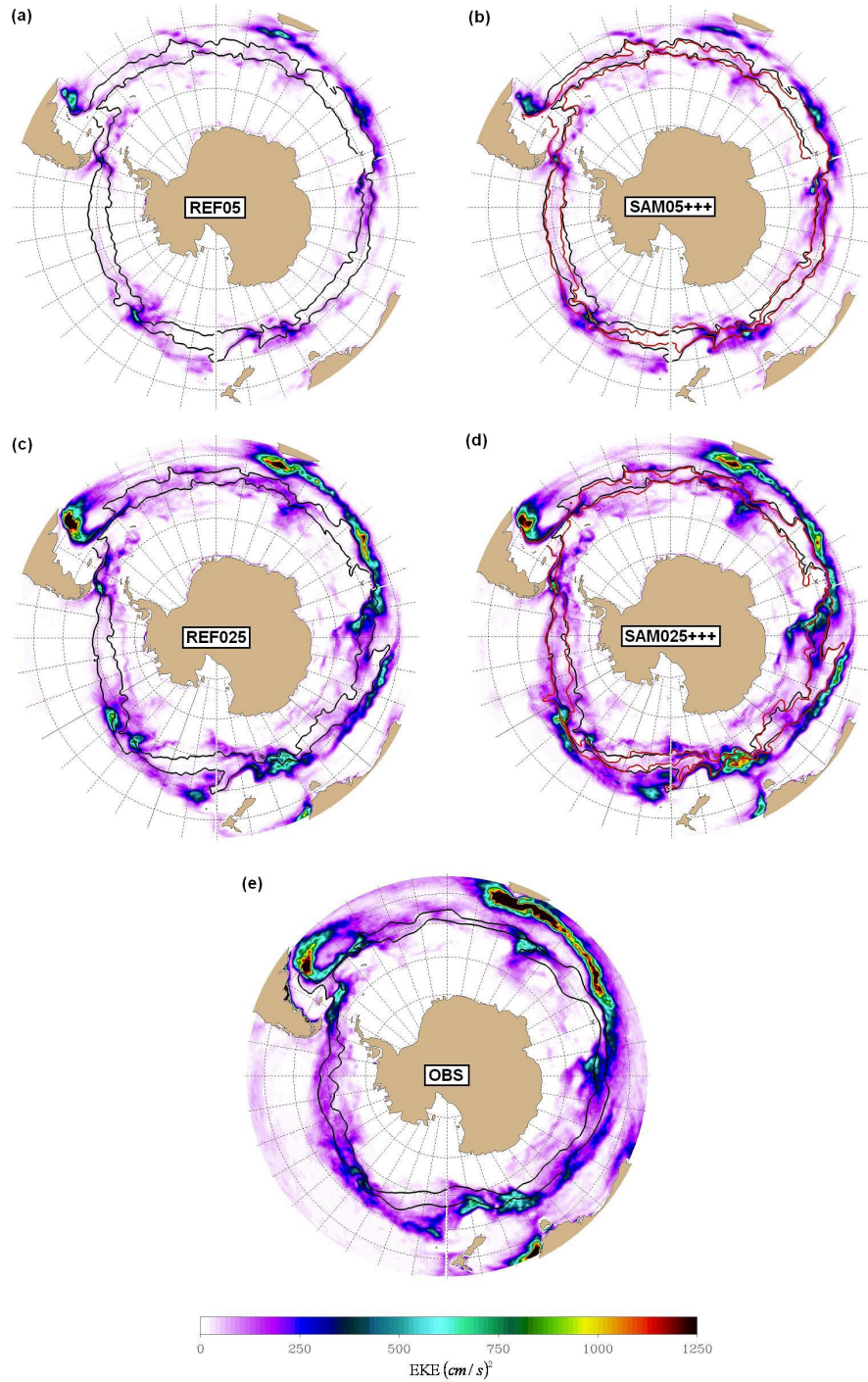
FIG. 2. Mean EKE over 1992–2002 in (cm² s⁻²) from (a-d) the simulations at 10 m and (e) the TOPEX-POSEIDON satellite data. Satellite data were regrided to 0.25° resolution for comparison. Also shown are mean positions of the PF and SAF (a-d) for 1995–2004 computed in simulations following Sallée et al. (2008) and (e) from Orsi et al. (1995). In (b) and (d), black contours correspond to front locations in REF05 and REF025 while red contours are for front locations in SAM05+++ and SAM025+++.

41
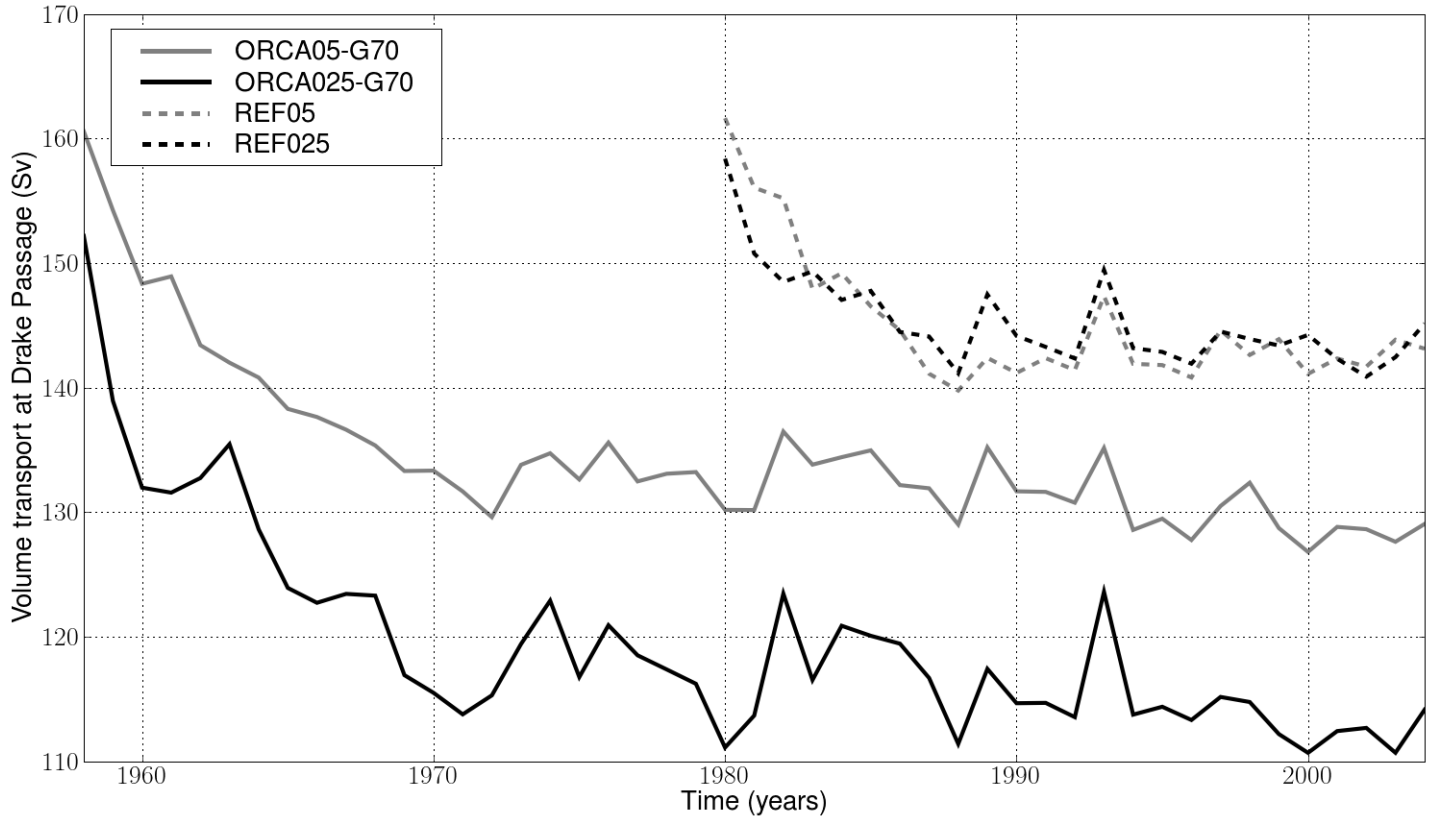
FIG. 3. Time series of annual mass transport at Drake Passage (in Sv) for the DRAKKAR global simulation at 0.5° (grey solid line) and 0.25° (black solid line) as well as the regional reference simulations at 0.5° (dash grey line) and 0.25° (black dashed line).
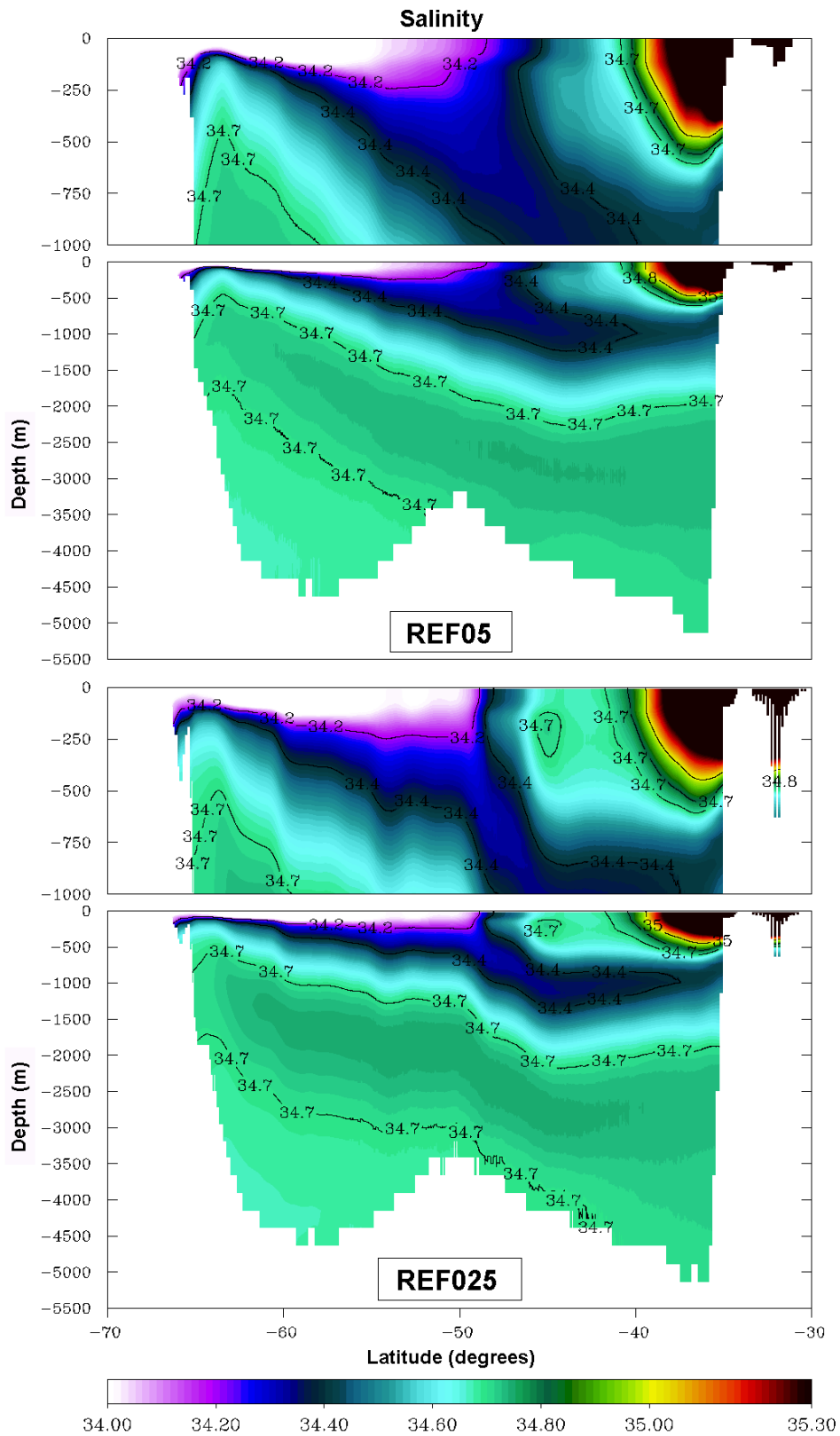
FIG. 4. Mean simulated salinity (1995–2004) along a meridional section at 115°E in the REF05 (top panel) and REF025 (bottom panel) with a zoom on the upper 1000 m. Solid black contours indicate some salinity contours. The colorbar indicates salinity on the practical salinity scale.
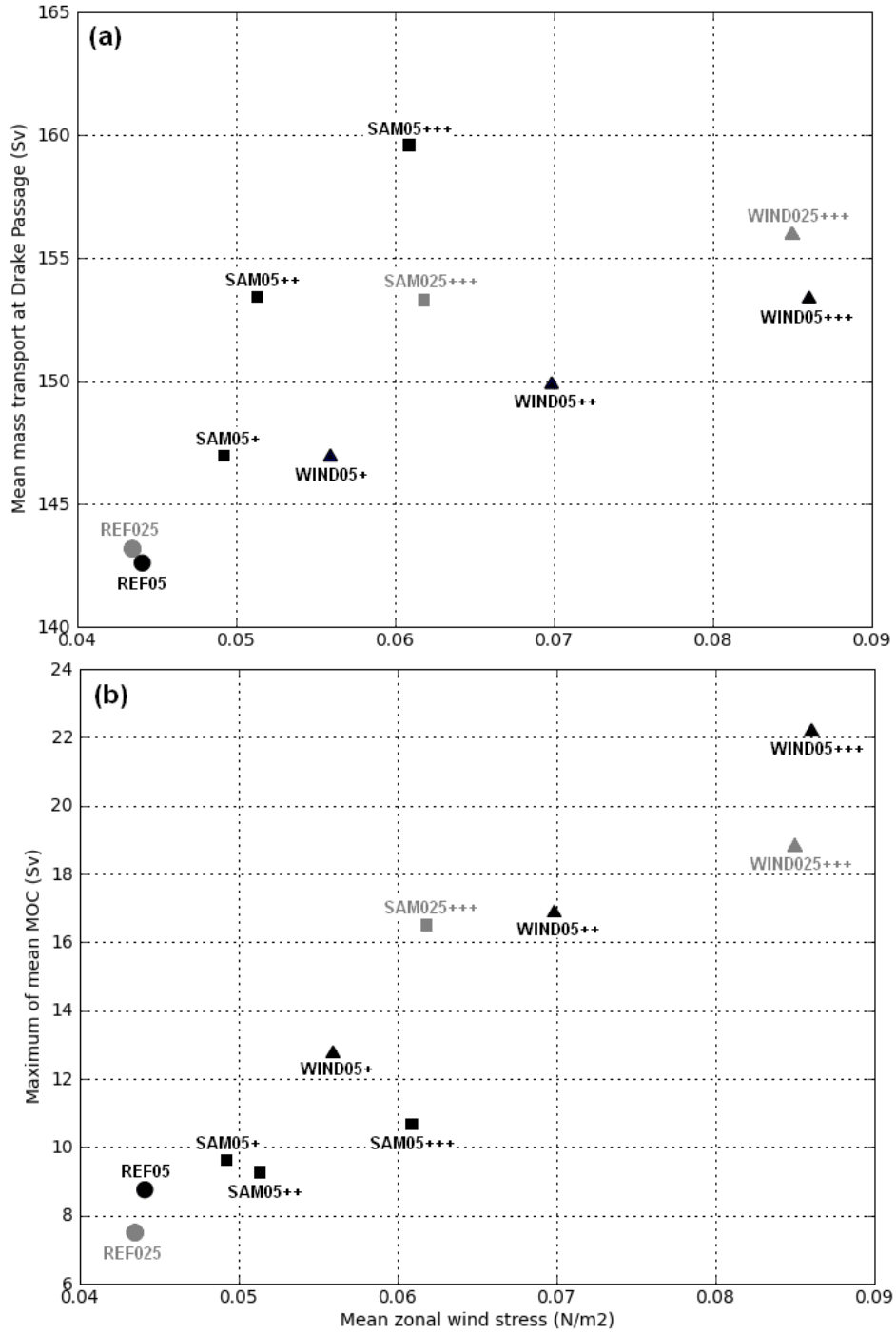
FIG. 5. (a) Mass transport at Drake Passage (in Sv) and (b) Maximum transport of the subpolar cell between 40°S and 55°S (in Sv), each given as the 1995–2004 mean and plotted against mean zonal wind stress in N m^{-2} for the same period. Symbols indicate the series of simulations: REFxxx (circles), WINDxxx (triangles) and SAMxxx (squares). Colors indicate resolution: 0.5° (black) and 0.25° (grey).

44
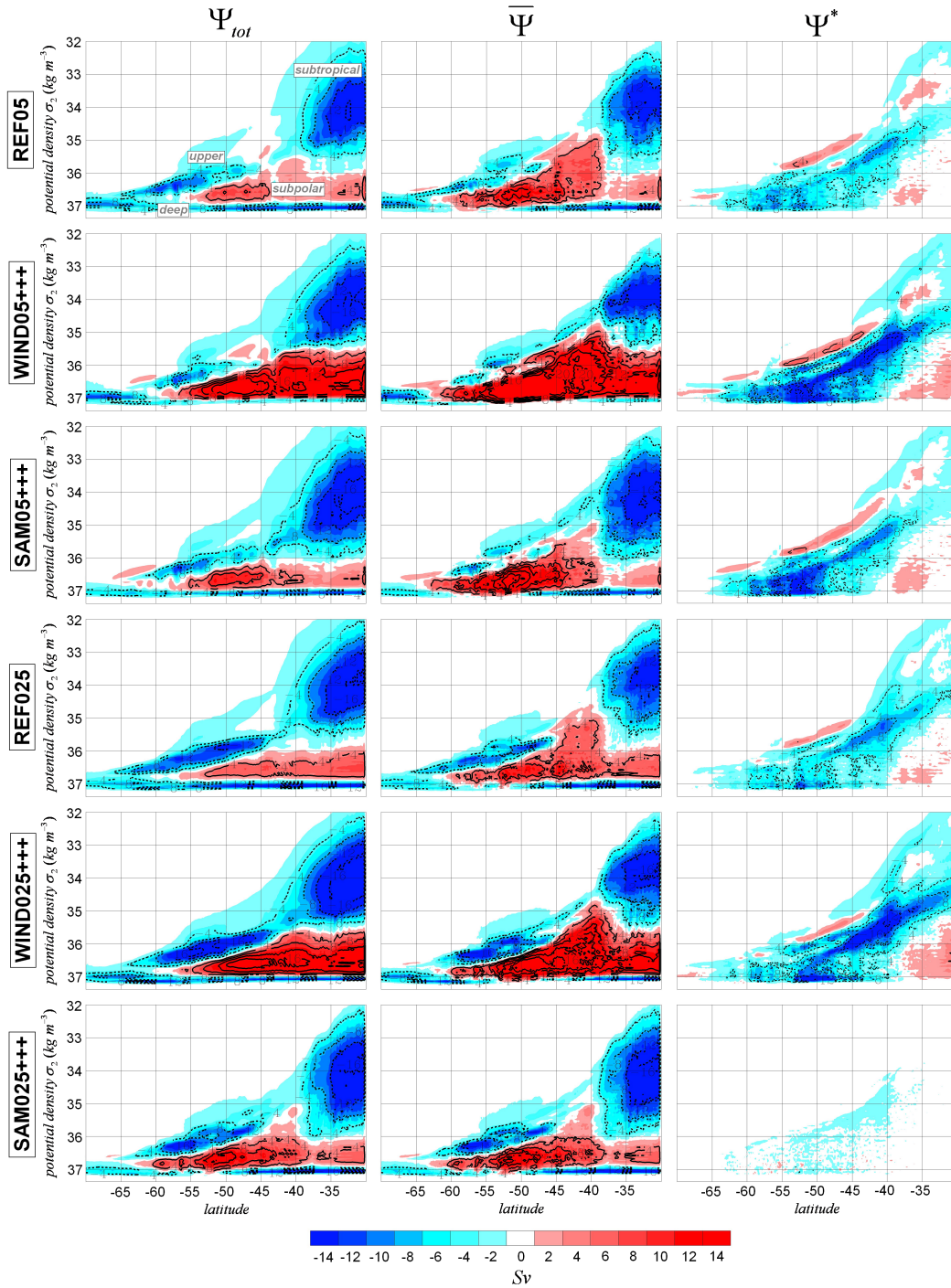
FIG. 6. The MOC (in Sv) in σ_2 potential density coordinates for (left) the total circulation Ψ_{tot}, (middle) the mean Eulerian circulation $\overline{\Psi}$, and (right) the transient eddy-induced circulation Ψ^*. Simulations are indicated for from top to bottom as REF05, WIND05+++, SAM05+++, REF025, WIND025+++ and SAM025+++. Red cells indicate clockwise flow while blue cells indicate counter-clockwise flow. (Top left panel, in grey) Nomenclature of the four distinct cells are given and are described in section 3.b.

45
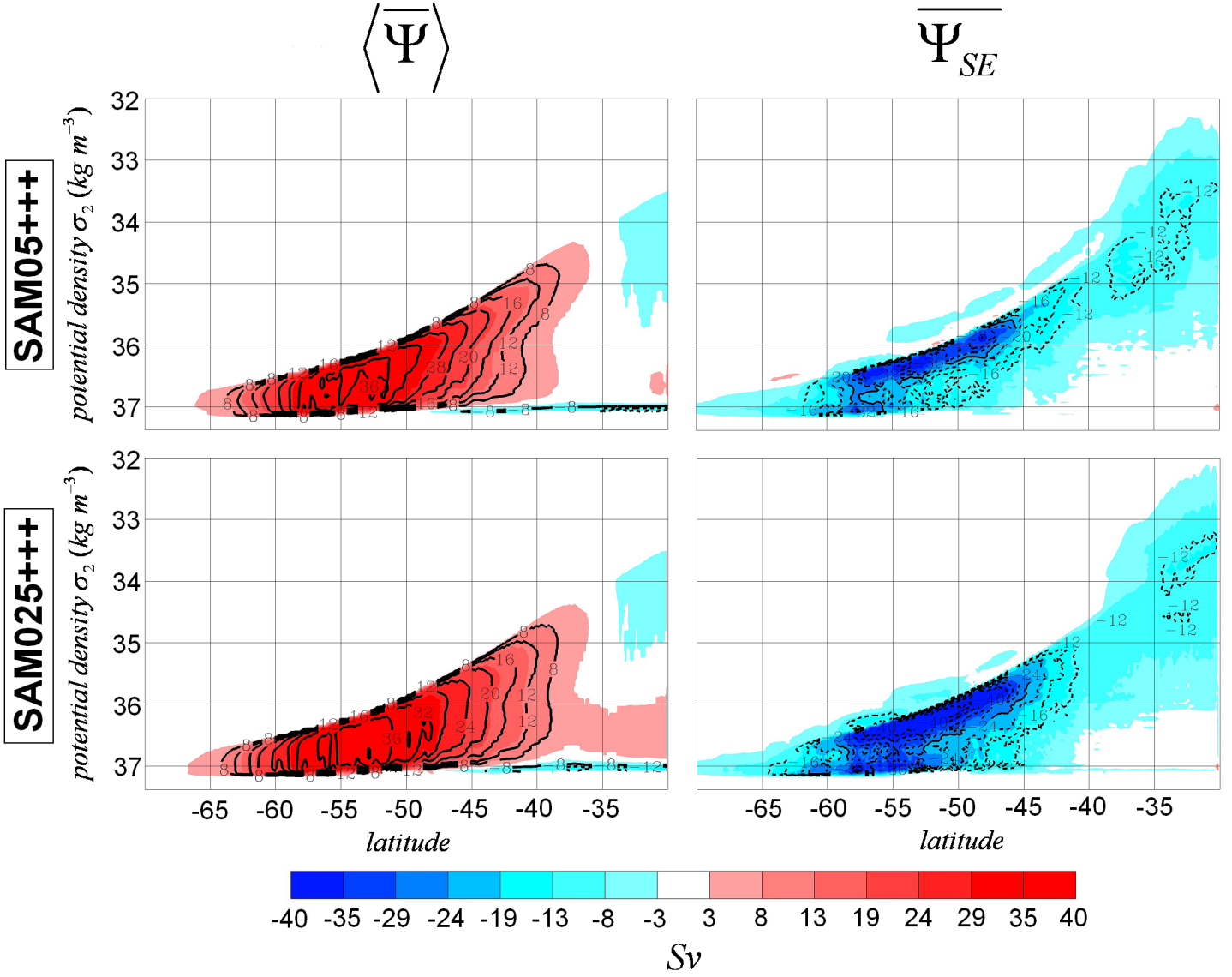
FIG. 7. The mean Eulerian circulation (in Sv) in σ_2 potential density coordinates separated into (left) zonal-average mean Eulerian circulation $<\overline{\Psi}>$ and (right) the standing eddy-driven circulation $\overline{\Psi_{SE}}$ for SAM05+++ (top) and SAM025+++ (bottom). Red indicates clockwise flow and blue indicates counterclockwise flow.
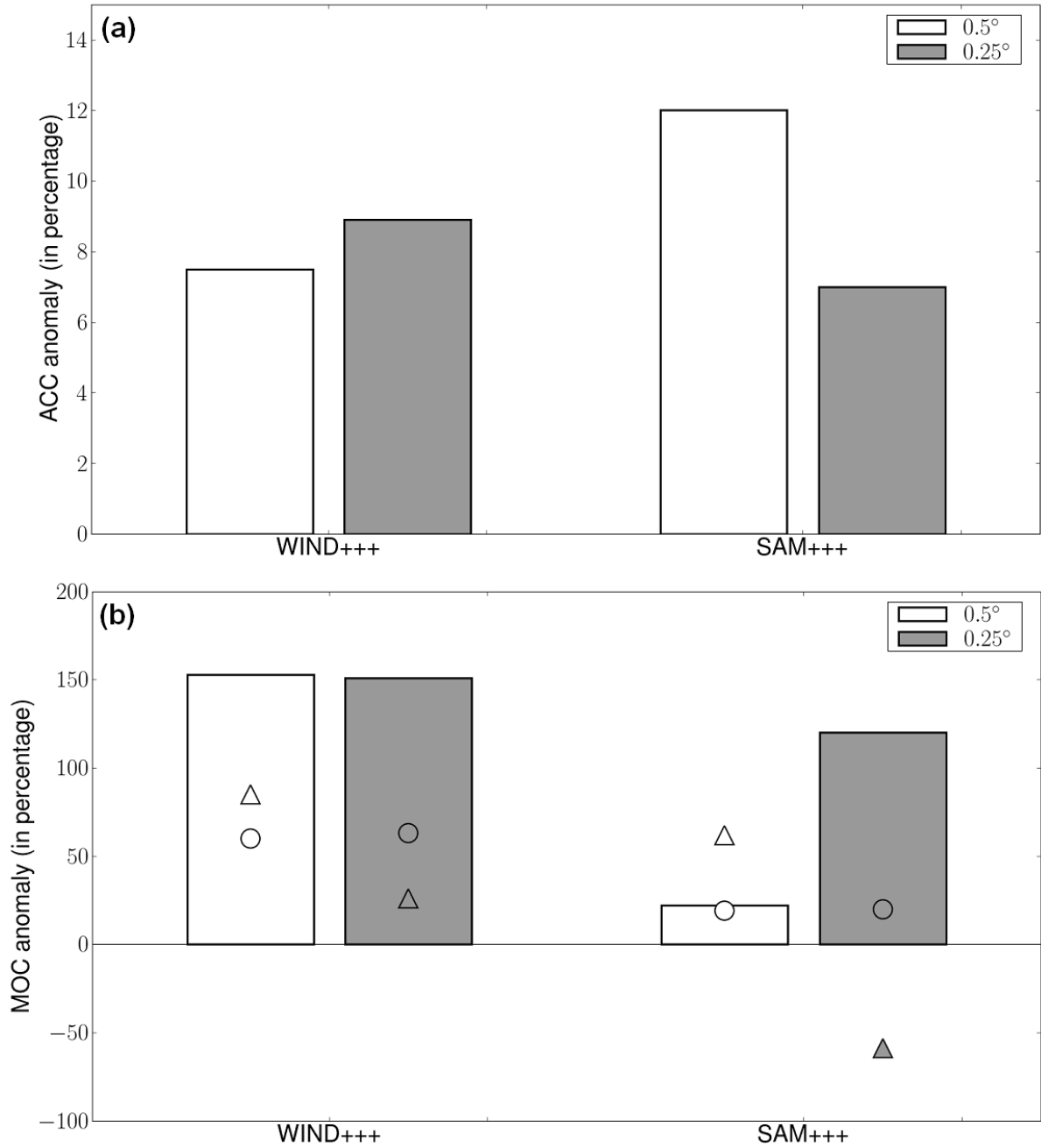
FIG. 8. Anomalies for (a) Drake Passage transport and (b) MOC subpolar cell intensity for WIND+++ and SAM+++ simulations at 0.5° and 0.25° resolutions relative to the respective reference simulations (REF05 and REF025), given in percent for the 1995–2004 mean. In (b) Vertical bars represent anomalies in Ψ_{tot} (MOC), circles correspond to anomalies in $\overline{\Psi_{SE}}$ (standing-eddy component), and triangles indicate anomalies in Ψ^* (transient-eddy component).
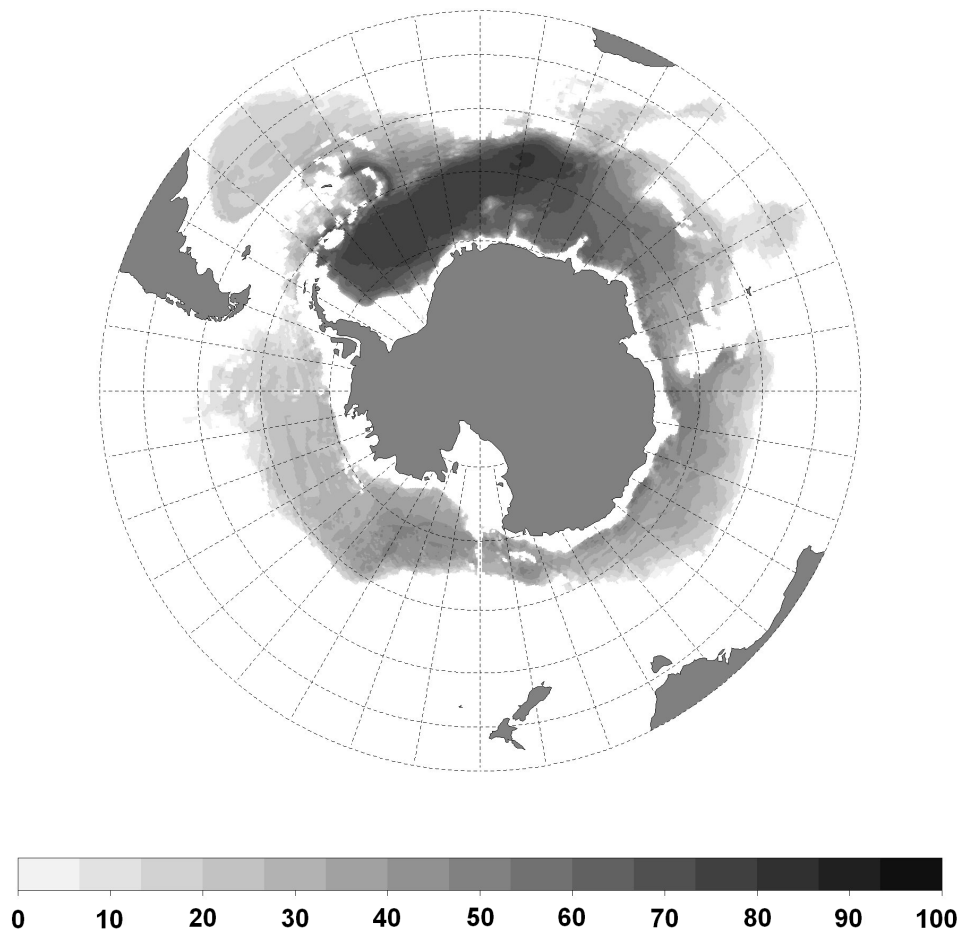
47

FIG. 9. Percent of water depth that is restored with a time scale of less than ten years, i.e., with a total restoring coefficient of $\frac{M(x,y,z)}{\tau} > 3.17 \times 10^{-9}\,\text{s}^{-1}$, corresponding to a mask coefficient M(x,y,z) > 0.2 and a restoring time scale $\tau = 2$ years.

List of Tables

TABLE 1. Comparison of various eddying model configurations in terms of grid type (column 2) and grid-cell size at 60°S (column 3). A Mercator grid is isotropic, i.e., dy is refined as dx decreases poleward. Studies using these models to study the sensitivity of Southern Ocean circulation to winds are indicated in the final column.

Model	*Grid type*	*dy*	*Reference*
ORCA2-LIM	Mercator	100 km	(Lefebvre and Goose 2005)
PERIANT05	**Mercator**	**28 km**	**this study**
MESO 1/2°	Mercator	28 km	(Hallberg and Gnanadesikan 2006)
OCCAM 1/4°	lon,lat	27 km	-
UVic ESCM 0.2°x0.4°	lon,lat	22 km	(Spence et al. 2010)
PERIANT025	**Mercator**	**14 km**	**this study**
CM2.4	Mercator	14 km	(Farneti et al. 2010)
MESO 1/4°	Mercator	14 km	(Hallberg and Gnanadesikan 2006)

TABLE 2. Main characteristics of simulations: horizontal resolution, parameters of the synthetic forcing (α and β are the constants defined in the equation (1) and 1 std(I_{SAM}) = 0.993; I_{SAM} being the SAM index), ACC mean position is estimated from the Polar Front (PF) and the Subantarctic Front (SAF) mean positions (see section 3.a.1), the shift of the mean position relative to the control simulations (REFxxx), and the width of the ACC (distance between the PF and the SAF mean positions). The last line corresponds to ACC mean position and width estimated from climatological observations (Orsi et al. 1995).

Simulation	Resolution	α	β [std(SAM)]	ACC	Shift	Width
REF05	0.5°	1	0	51.1°S	-	7.1°
WIND05+	-	1.1	0	50.1°S	1.0°N	5.3°
WIND05++	-	1.2	0	49.7°S	1.4°N	4.8°
WIND05+++	-	1.3	0	49.4°S	1.7°N	4.3°
SAM05+	-	1	0.5	51.3°S	0.2°S	6.6°
SAM05++	-	1	1	50.7°S	0.4°N	5.2°
SAM05+++	-	1	2	50.9°S	0.2°N	4.9°
REF025	0.25°	1	0	50.3°S	-	5.7°
WIND025+++	-	1.3	0	49.2°S	1.1°N	4.1°
SAM025+++	-	1	2	50.6°S	0.3°S	5.3°
Orsi et al. (1995)	-	-	-	53.1°S	-	3.7°